Electronic Supporting Information

N skeleton-regulated cobalt phthalocyanine promote polysulfides adsorption and redox kinetics

Jiaqi Zhao,[a] Zhanwei Xu,[*a] Yujiao Zhang,[b] Kai Yao,[c] Liang Li,[a] Hang Niu,[a] Jiayin Li,[a] Zhi Li[*d]

School of Materials Science and Engineering, Shaanxi Key Laboratory of Green Preparation and Functionalization for Inorganic Materials, Shaanxi University of Science and Technology, Xi'an, 710021, PR China
E-mail: xuzhanwei@sust.edu.cn

Department of Chemical and Materials Engineering, University of Alberta, Edmonton Alberta T6G 2 M9, Canada
E-mail: zhi.li@ualberta.ca

Author contributions

Jiaqi Zhao: investigation, data curation, visualization, writing-original draft of experimental part, Writing-review & editing. Zhanwei Xu: funding acquisition, supervision. Yujiao Zhang: Funding acquisition. Kai Yao: investigation. Liang Li: validation. Hang Niu: validation. Zhi Li: supervision, writing-review & editing.

S1. Experimental Section

S1.1. Raw Material

$CoCl_2•6H_2O$ and $(NH_4)_6Mo_7O_{24}•4H_2O$ were purchased from Sinopharm Chemical Reagent Co., Ltd. Phthalic anhydride and pyridine-2,3-dicarboxylic acid were purchased form shanghai Aladdin Biochemical Technology Co., Ltd. pyrazine-2,3-dicarboxylic was purchased from Tokyo chemical industry Co., Ltd. Reduced graphene oxide (rGO) was provided by Shaanxi Coal Chemical Industry Technology, Research Institute co., Ltd.

S1.2. Synthesis of CoPc/rGO, CoTAP/rGO and CoPTpz/rGO

0.2 g rGO, 0.31 g $CoCl_2•6H_2O$, 0.06 g $(NH_4)_6Mo_7O_{24}•4H_2O$, 0.6 g urea and 0.41 g phthalic anhydride was dispersed in 100 ml deionized water for 24 h stirring and ultrasonication. Then the preform was obtained by Freeze-drying abovementioned mixture. CoPc/rGO were synthesized by heating precursor to 140^oC for 30 min and then increased temperature to 270^oC for 2 h. Followed by a series of purification procedure, CoPc/rGO composite were obtained. The CoTAP/rGO and CoPTpz/rGO were synthesized by change 0.41 g of phthalic anhydride to pyridine-2,3-dicarboxylic acid and pyrazine-2,3-dicarboxylic in the same method of CoPc/rGO.

S1.3. Fabrication of CoPc/rGO, CoTAP/rGO and CoPTpz/rGO modified separators

The CoPc/rGO, Acetylene black(AB) and Polyvinylidene Fluoride (PVDF) powder were weighed based on the weight ratio of 8:1:1. After fully grinding, they were dissolved into N-Methylpyrrolidone(NMP) to prepare the uniformly slurry. Then the slurry was blade coating on the PP substrate. At last, the obtained CoPc/rGO@PP was cut into discs with a diameter of 19 mm. The CoTAP/rGO and CoPTpz/rGO modified separators were prepared under the same conditions.

S1.4. Fabrication of Cathodes and Cells

The cathodes consist of 80 wt % sulfur/acetylene black (AB), 10 wt % AB, and 10 wt % polyvinylidene fluoride (as a binder). The cathode slurry was coated on aluminum foil followed by drying at 70 °C for 12 h in a vacuum oven. The areal sulfur mass loading is about 1.781 mg cm^{-1}. Coin cells were assembled in a glovebox with a Li chip as the anode, Celgard 2500 as the separator, 1.0 M LiTFSI in DME/DOL = 1:1 vol % with 1.0 wt % $LiNO_3$ as the electrolyte, CoPc/rGO, CoTAP/rGO and CoPTpz/rGO as the interlayer between the separator and cathode. The areal mass loading is about 0.93 mg cm^{-1}

S1.5. Characterization

Raman measurements were performed on an InVia instrument using 532 nm diode-pumped solid-state laser. Fourier transform infrared (FT-IR) spectroscopy was performed using a Bruker Alpha VECTOR-22 type analyzer.

S1.7. Li_2S nucleation tests

The assembled cells were firstly galvanostatically discharged to second discharge plateaus, usually 2.10 V under 0.1 C current, and subsequently held potentiostatically at 2.09 V until the current was below 0.01 mA for nucleation and growth of Li_2S. Based on Faraday's law, the nucleation/growth rate of Li_2S on diverse host surfaces was evaluated by collecting the whole energy was collected through *i-t* curves.

S1.8. Electrochemical characterizations

The standard CR2032-type coin cells were assembled in a glove box with Ar-filled, while the oxygen and moisture content are less than 0.1 ppm. The electrolyte was 1.0 M LiTFSI dissolved into mixed solvents of DOL and DME (v/v = 1:1) with 1 wt.% of $LiNO_3$. The amount of the electrolyte added dropwise to a coin cell is controlled at around 20 μL. To control the loadings of sulfur in the sulfur cathode, the same process was repeated several times. The regular sulfur loading is 1.0~1.5 mg cm^{-2}. The cyclic voltammetry (CV) curves were performed on princeton electrochemical workstation with various scan rates from of 0.1-0.5 mV s^{-1} from 1.7 to 2.8 V and the electrochemical impedance spectra (EIS) was tested on electrochemical workstation in a frequency range of 100 kHz to 0.01 Hz for Li-S cells. All the electrochemical tests were performed at room temperature. The GITT test, cycling performance and rate properties of the batteries were characterized using LAND CT2001A battery test system. All the electrochemical tests were performed at room temperature.

Calculation of Li^+ diffusion coefficient

The Li^+ diffusion coefficient was calculated based on the CV curves with various scan rates by the Randles-Sevcik equation:

$$I_P = \left(2.69 \times 10^5\right) n^{1.5} A D^{0.5} C v^{0.5} \quad \text{(S1)}$$

Where I_p designates the current peak, while n, A , and ν are the numbers of electrons transferred during the reaction, the electrode's surface area, and the scan rate. The values of C and D correspond to the concentration and diffusion coefficient of Li^+, respectively. The slope is in direct ratio to D_{Li^+}.

Calculation Details of Relative Activation Energy (E_a).

$$E_a = E_a^0 - \frac{RT}{b}\varphi(Ox/Red)_{IR} \quad \text{(S2)}$$

where E_a and E_a^0 refer to the activation energy and intrinsic activation energy, respectively. R is the molar gas constant, T represents the thermodynamic temperature, b is the slope of the Tafel curve, and φ is the irreversible potential in the reduction process.

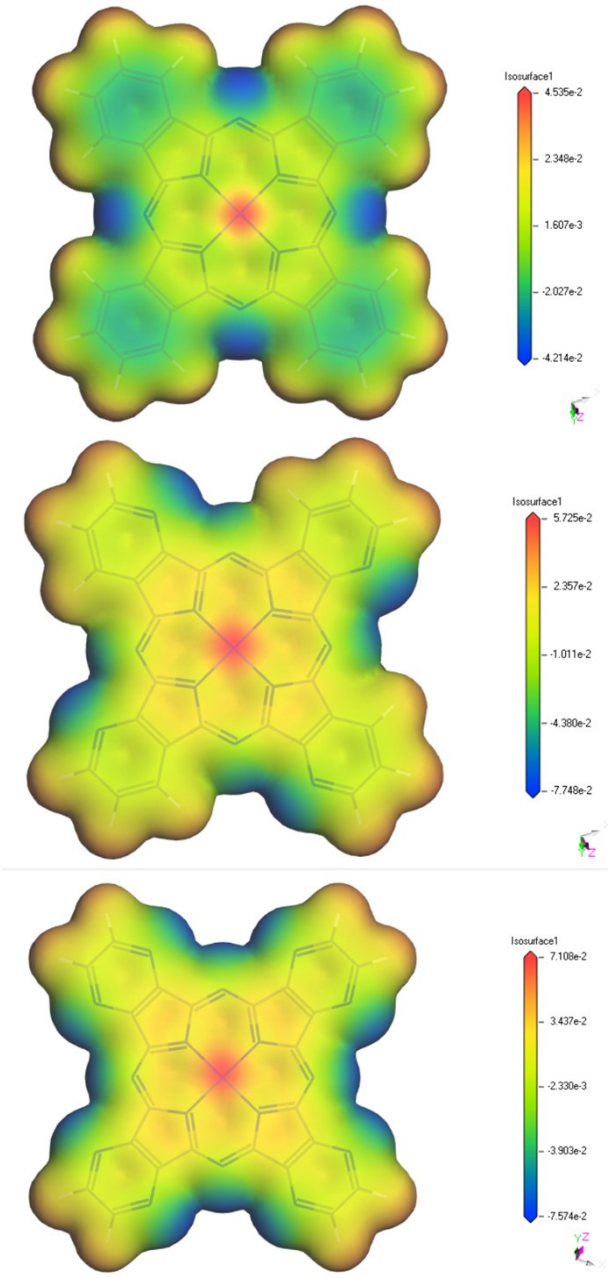

Fig. S1 The EPS mapping of CoPc, CoTAP and CoPTpz molecules.

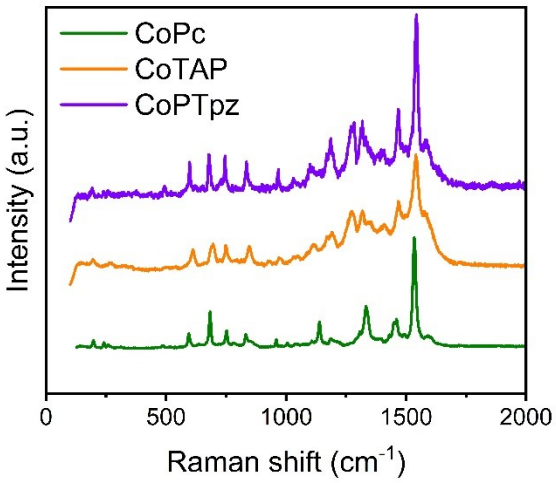

Fig. S2 the Raman spectra of CoPc, CoTAP and CoPTpz

The peak at around 1344 cm^{-1} is overlapped by two peaks from the lattice defect of rGO (1344 cm^{-1}) and the C-C pyrrole stretch of phthalocyanine (1340 cm^{-1}), respectively. And the peak at around 1526 cm^{-1} is assigned to the C-N aza-group stretch.

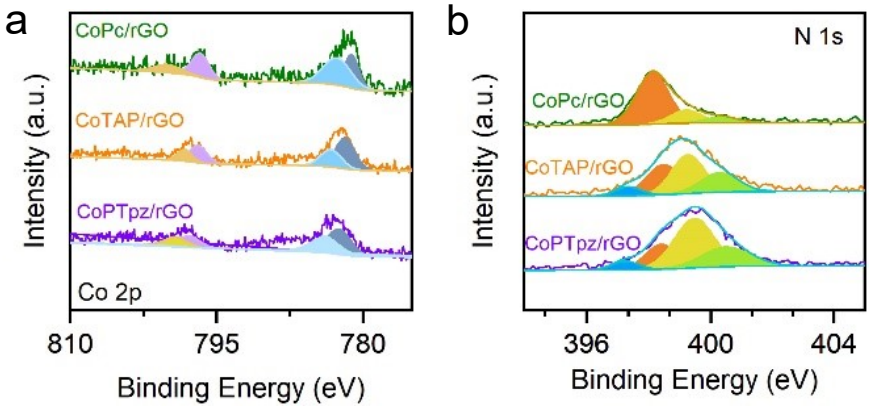

Fig. S3. XPS spectra of CoPc/rGO, CoTAP/rGO, and CoPTpz/rGO about (a) Co 2p and (b) N 1s.

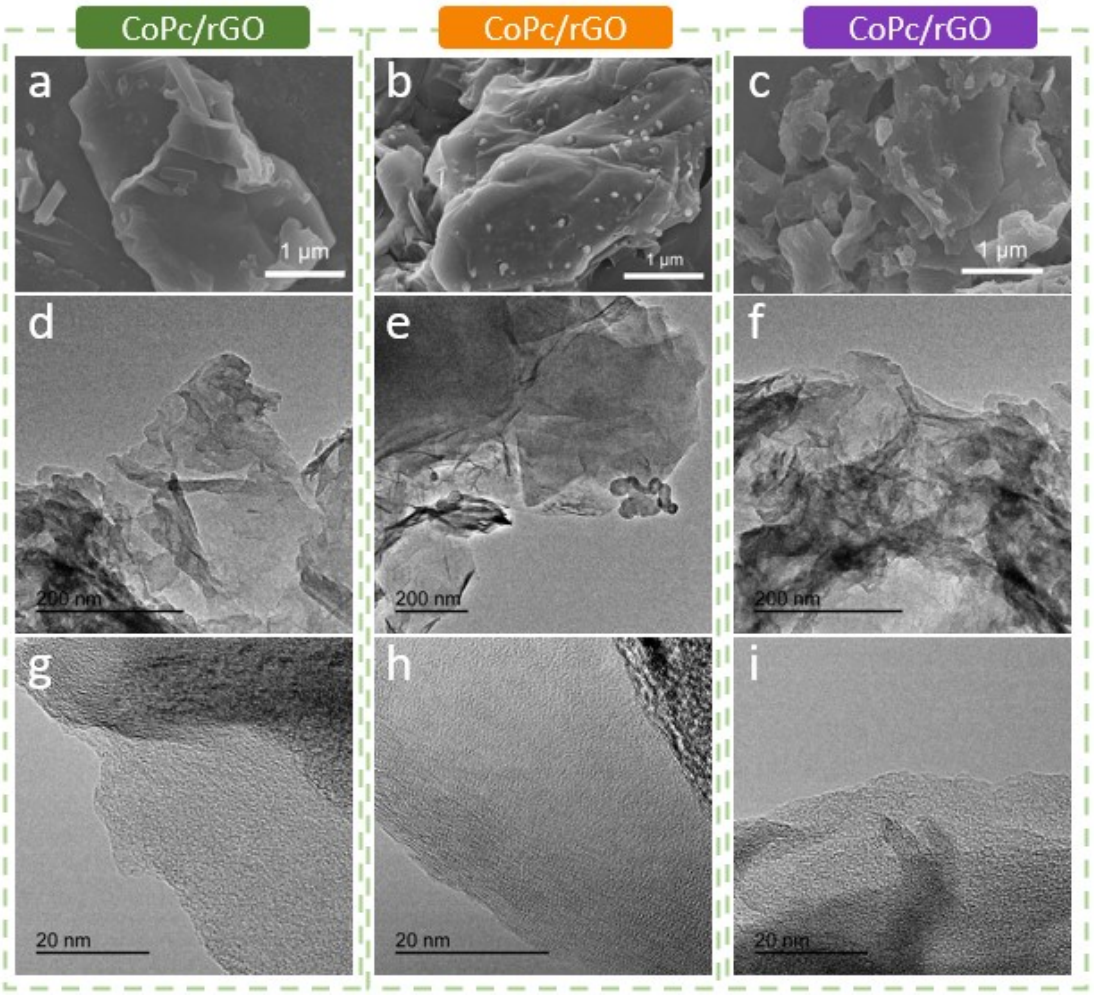

Fig. S4 The SEM images of (a) CoPc/rGO, (b) CoTAP/rGO, (c) CoPTpz/rGO. The TEM images of (d) CoPc/rGO, (e) CoTAP/rGO, (f) CoPTpz/rGO. The HRTEM images of (g) CoPc/rGO, (h) CoTAP/rGO, (i) CoPTpz/rGO.

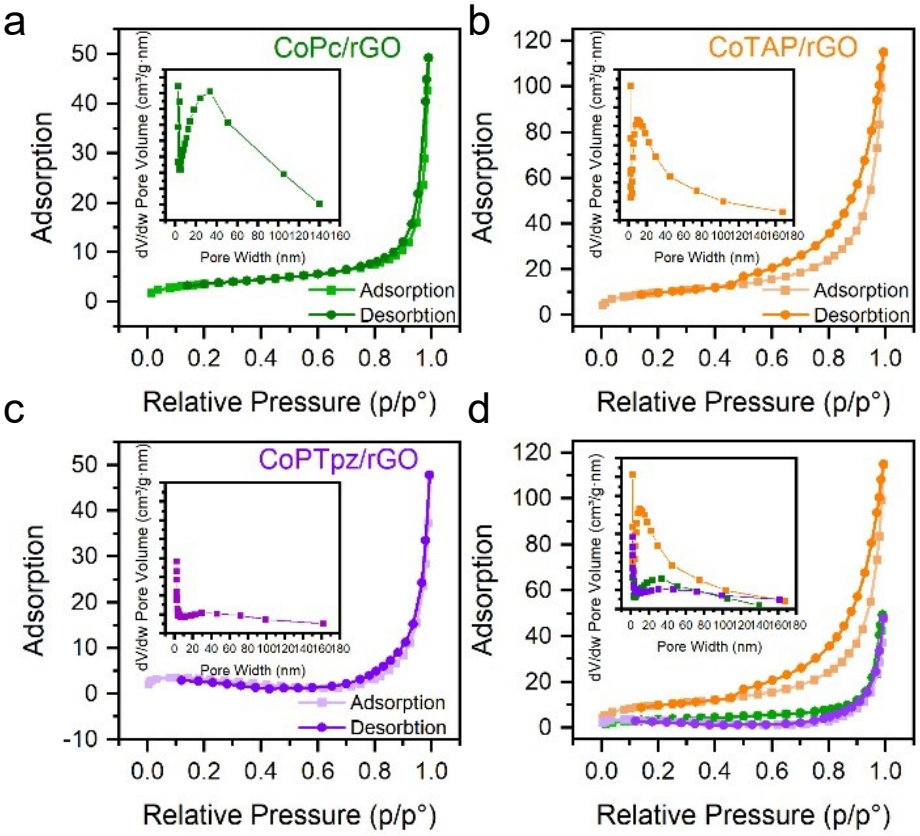

Fig. S5. Adsorption and desorption curves of (a) CoPc/rGO, (b) CoTAP/rGO, (c) CoPTpz/rGO, and (d) all samples.

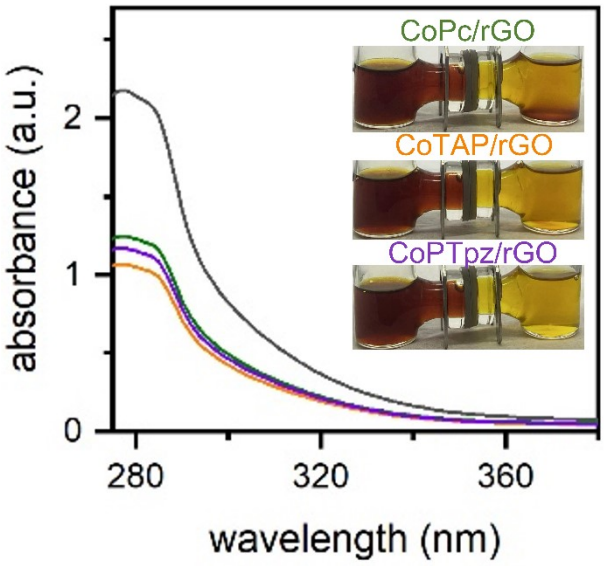

Fig. S6. The penetration test and UV-vis spectra about CoPc/rGO, CoTAP/rGO, and CoPTpz/rGO separators towards Li_2S_6.

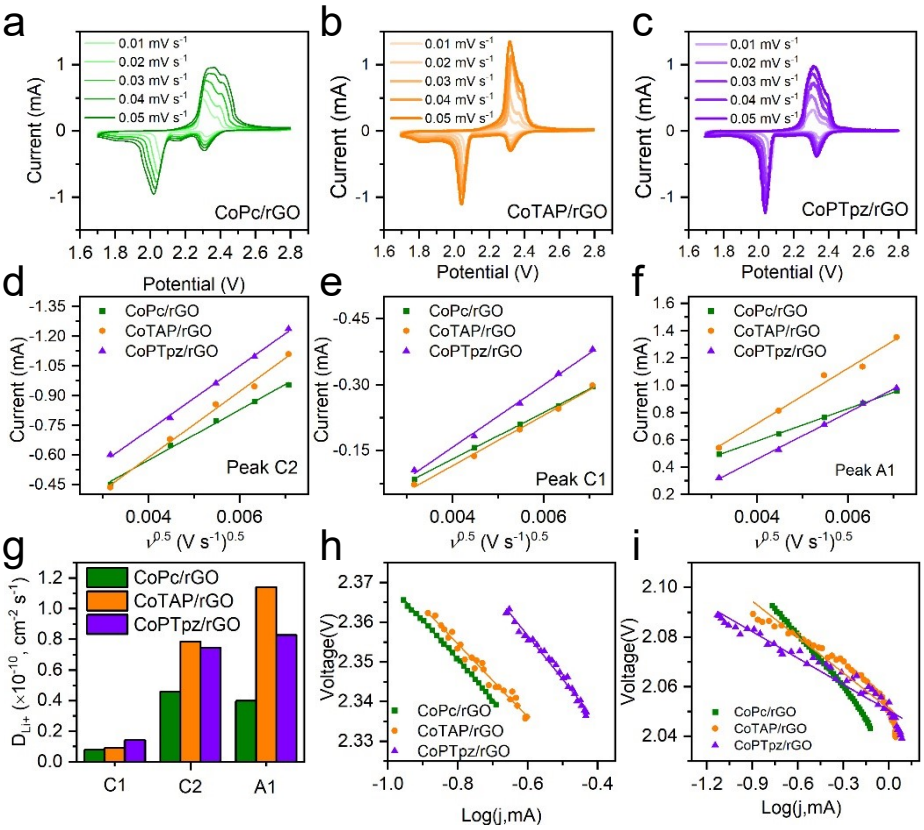

Fig. S7. CV curves at scan rates from 0.01 - 0.05 mV s^{-1} of (a) CoPc/rGO, (b) CoTAP/rGO and (c) CoPTpz/rGO. (d-f) Plot of the currents of all CV redox peaks versus the square root of the scan rates. (g) the calculated D_{Li+} of various peaks in CV curves. (h-i) Corresponding tafel plots of peak C1 and C2

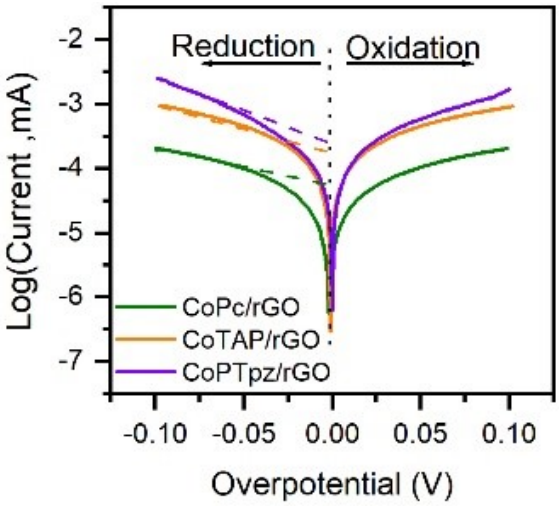

Fig. S8. Tafel plots of S//S symmetric cells.

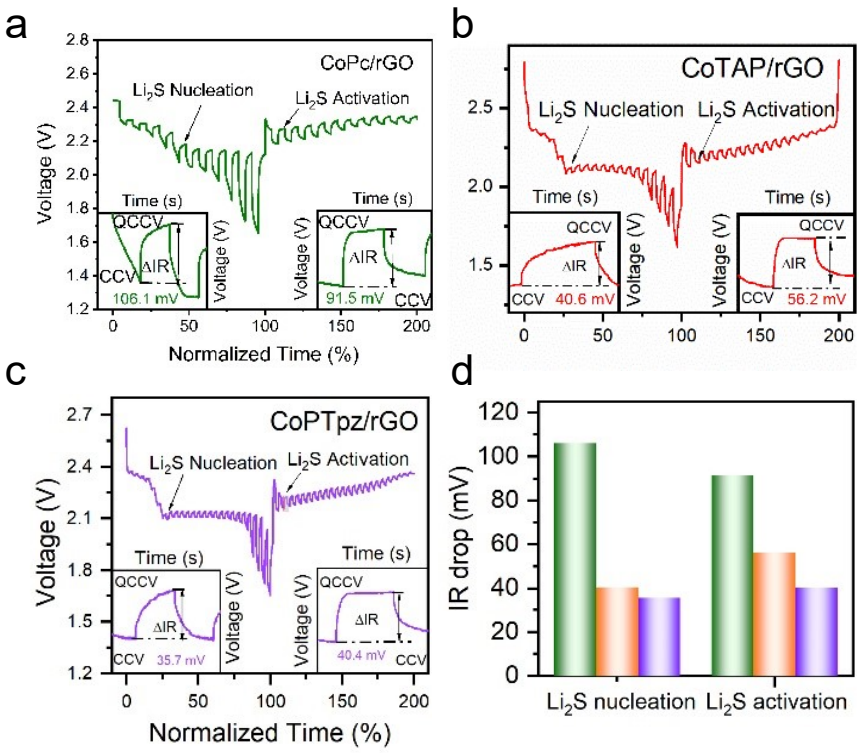

Fig. S9 The GITT curves of (a) CoPc/rGO and (b) CoTAP/rGO. (c) CoPTpz/rGO. (d) the IR drops at Li_2S activation and nucleation.

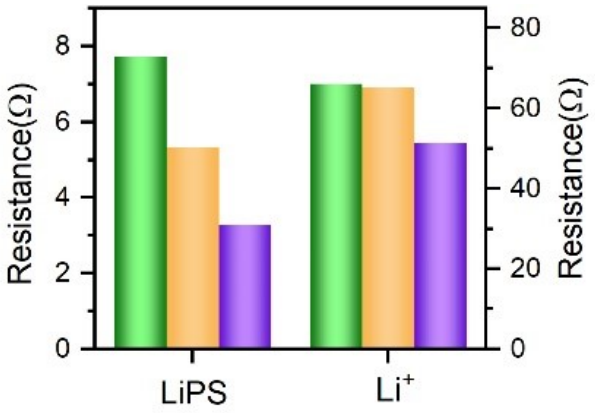

Fig. S10 the diffusion resistance of LiPS and Li^+.

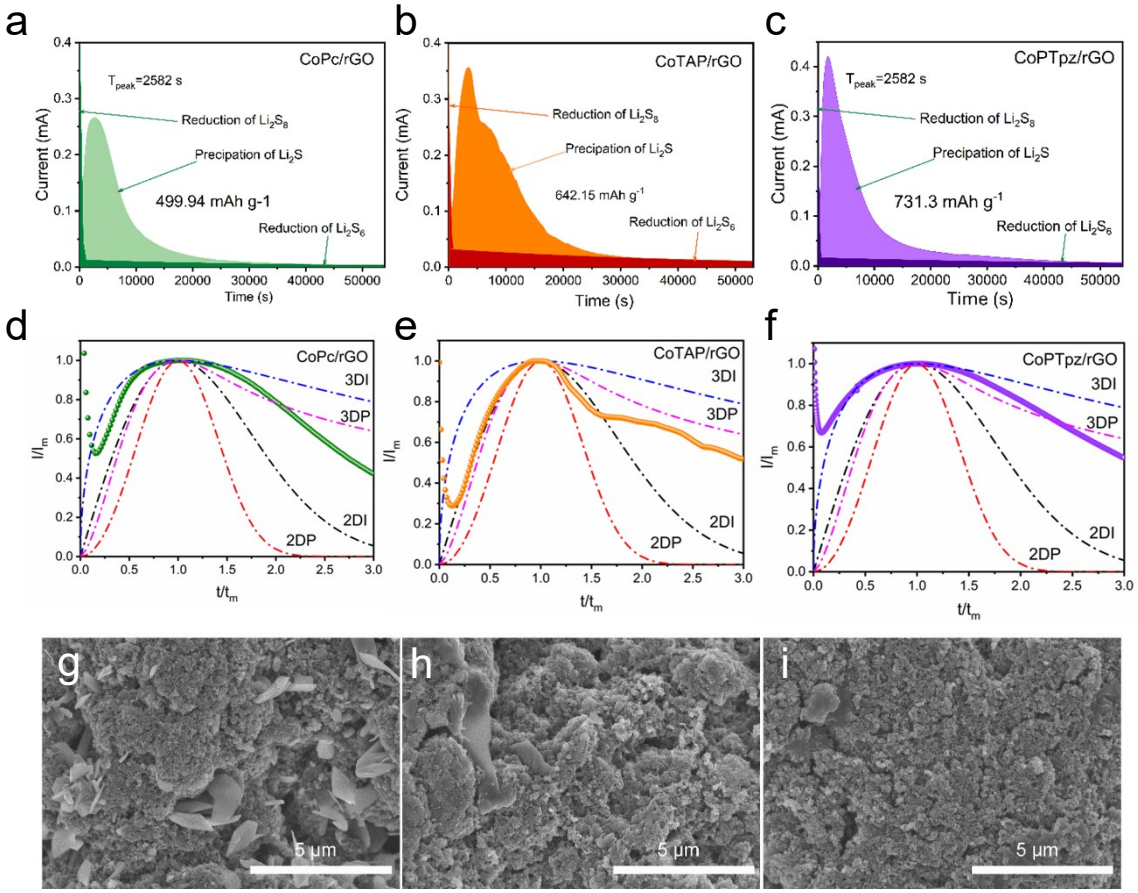

Fig. S11 Potentiastatic Li_2S deposition curves of (a) CoPc/rGO, (b) CoTAP/rGO and (c) CoPTpz/rGO at 2.09 V. Corresponding dimensionless Current–time transients in comparison with theoretical models of (d) CoPc/rGO, (e) CoTAP/rGO and (f) CoPTpz/rGO separator. SEM images of final Li_2S deposition morphology of (g) CoPc/rGO, (h) CoTAP/rGO and (i) CoPTpz/rGO.

The deposition curves of various catalysts were measured at a stable potential of 2.09 V after discharging to 2.10 V.

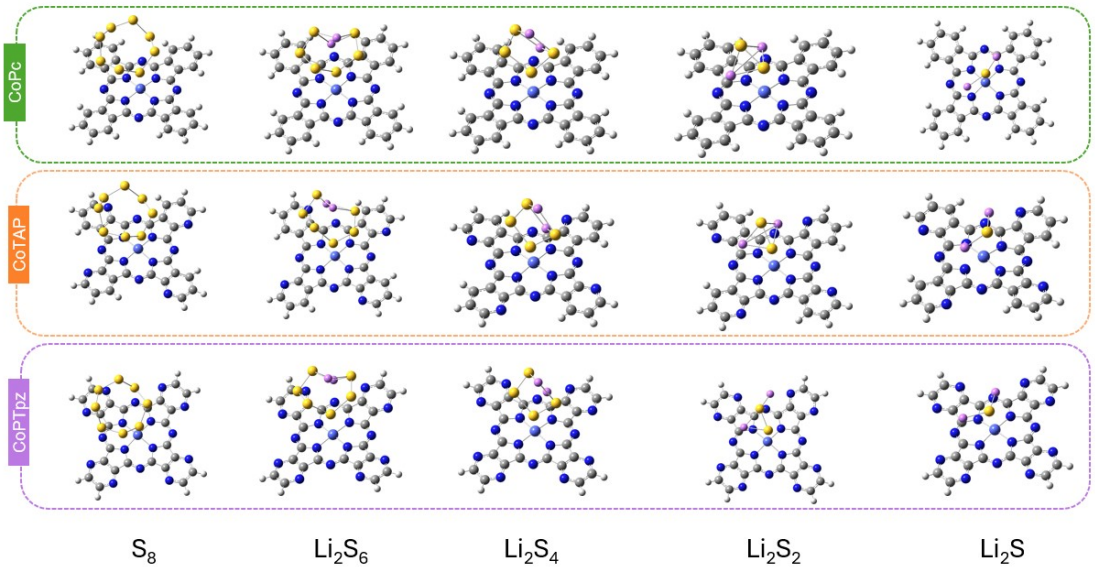

Fig. S12. Optimized adsorption model of CoPc, CoTAP and CoPTpz with various sulfur species.

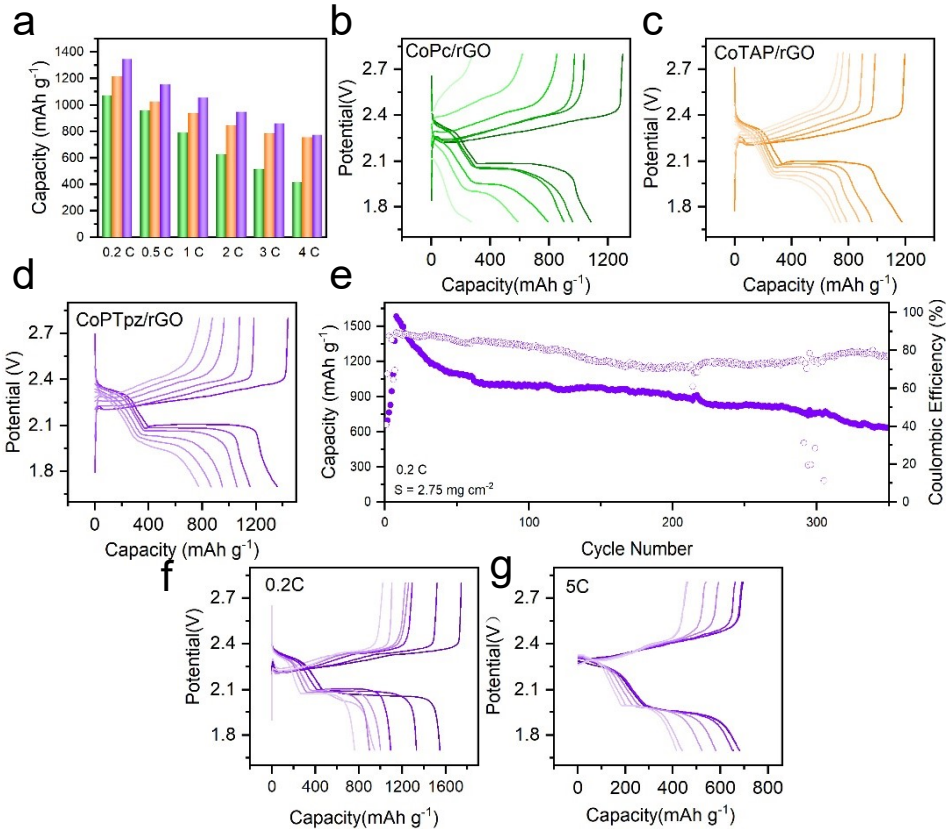

Fig. S13. The charge discharge curves of (a) CoPc/rGO, (b) CoTAP/rGO and (c) CoPTpz/rGO. (d) discharge capacity of various separators under 0.2 C-4 C. (e) The cycle performance of CoPTpz/rGO at 0.2 C with 2.75 mg cm^{-2} sulfur loading. The charge discharge curves of CoPTpz/rGO (f) at 0.2 C with 2.75 mg cm^{-2} sulfur loading, (g) at 5 C rate.

Table S1 Raman shift of CoPc, CoTAP, and CoPTpz and their interpretation.

Raman Shift (cm^{-1})			interpretation
CoPc	CoTAP	CoPTpz	
198.5	195.2	192.5	Co-N stretch
595.3	596.1	598.2	Isoindole ring deformation
693.4	695.7	697.3	Macrocycle vibration
752.6	749.2	745.3	Macrocycle vibration
833	835.6	836	Macrocycle vibration
1138.7	1115.2	1099.3	C-H bending
1333.2	1320.2	1317.6	C-C pyrrole stretch
1533.4	1540.6	1542	C-N aza-group stretch

Table S2 The comparison of long-term cyclic performance with catalysts containing Co-N_4 sites.

Catalysts	Initial capacity (mAh g^{-1})	Reversible capacity (mAh g^{-1})	Cycle number	Sulfur loading (mg cm^{-1})	Decay rate (%)	Rate
This work	734	413	500	1.78	0.11%	5 C
CoTnPc[1]	1199	815	200	2.00	0.19%	0.5 C
Co–N_4@2D/3D[2]	957	690	500	1.00	0.065%	1 C
Co-$N_{4[3]}$	785	339	600	1.27	0.14%	1 C
Co-HTP/CG[4]	885	620	500	1.2-1.8	0.071%	1 C
($CoPc(OMe)_8$)[5]	1218	868	200	2.00	0.16%	0.5 C

.

All decay rates are calculated by the following equation:

$$DR = \left(1 - \left(\frac{Q_n}{Q_1}\right)^{\frac{1}{n}}\right) \times 100\% \quad \text{(S3)}$$

Where DR is decay rate, Q_n is discharge capacity after n cycles, Q_1 is initial discharge capacity, n is cycle number.

Reference

[1] Zhao, X.; Zhang, Y.; Liu, W.; Zheng, Z.; Fu, Z.; Chen, C.; Hu, C., Understanding the Impact of Peripheral Substitution on the Activity of Co Phthalocyanine in Sulfur Reduction Catalysis. *Adv. Funct. Mater.* 2024, *34* (13), 10.1002/adfm.202313107.

[2] Wang, R.; Wu, R.; Ding, C.; Chen, Z.; Xu, H.; Liu, Y.; Zhang, J.; Ha, Y.; Fei, B.; Pan, H., Porous Carbon Architecture Assembled by Cross-Linked Carbon Leaves with Implanted Atomic Cobalt for High-Performance Li-S Batteries. *Nano-Micro Lett.* 2021, *13* (1), 10.1007/s40820-021-00676-6.

[3] Li, Y.; Chen, Z.; Zhong, X.-Y.; Mei, T.; Li, Z.; Yue, L.; Yang, J.-L.; Fan, H. J.; Xu, M., Modulating the Coordination Environment of Co Single-Atom Catalysts: Impact on Lithium-Sulfur Battery Performance. *Adv. Funct. Mater.* 2024, 10.1002/adfm.202412279.

[4] Lv, Q.; Sun, Y.; Li, B.; Li, C.; Zhang, Q.; Wang, L., Metal-Organic Frameworks with Axial Cobalt-Oxygen Coordination Modulate Polysulfide Redox for Lithium-Sulfur Batteries. *Adv. Energy Mater.* 2024, 10.1002/aenm.202403223.

[5] Zhao, X.; Xu, Y.; Qiu, T.; Zhang, Y.; Liu, W.; Chen, C.; Biggs, M. J.; Hu, C., Enhanced Li bonds enable bidirectional sulfur catalysis by a molecular Co-N4 catalyst for lithium-sulfur

batteries. *Energy Storage Mater.* 2024, *72*, 10.1016/j.ensm.2024.103728.